Electronic Supplementary Material (ESI) for Physical Chemistry Chemical Physics.

Supporting Information: Applicability of Perturbed Matrix Method for Charge Transfer Studies at Bio/Metallic Interfaces: A Case of Azurin

Outi Vilhelmiina Kontkanen,[†] Denys Biriukov,[‡,†] and Zdenek Futera[*,†]

[†]*Faculty of Science, University of South Bohemia, Branisovska 1760, 370 05 Ceske Budejovice, Czech Republic.*

[‡]*Institute of Organic Chemistry and Biochemistry, Academy of Sciences of the Czech Republic, Flemingovo nam. 2, 16610 Prague 6, Czech Republic*

E-mail: zfutera@prf.jcu.cz(Z.F.)

Phone: +420-387-776-260

1 Azurin in solution

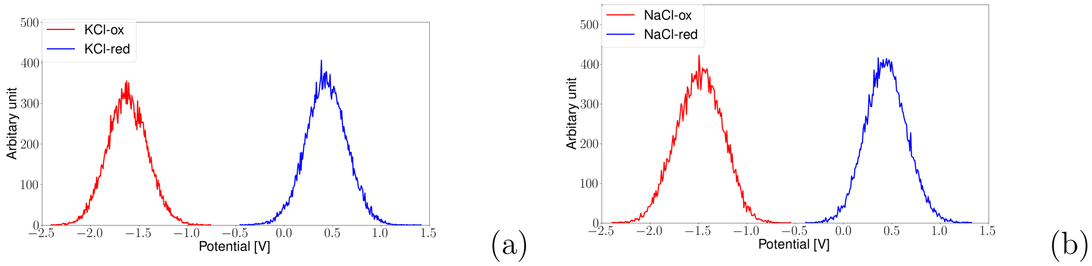

Figure S1: Histograms of the electrostatic potential [V] at the Cu atom in the reduced (blue) and oxidized (red) azurin in (a) KCl and (b) NaCl aqueous solutions. The potentials originate from the atomic point charges in the MM part of the model, i.e., the protein matrix and the water solution, as defined in the GolP-CHARMM force field.

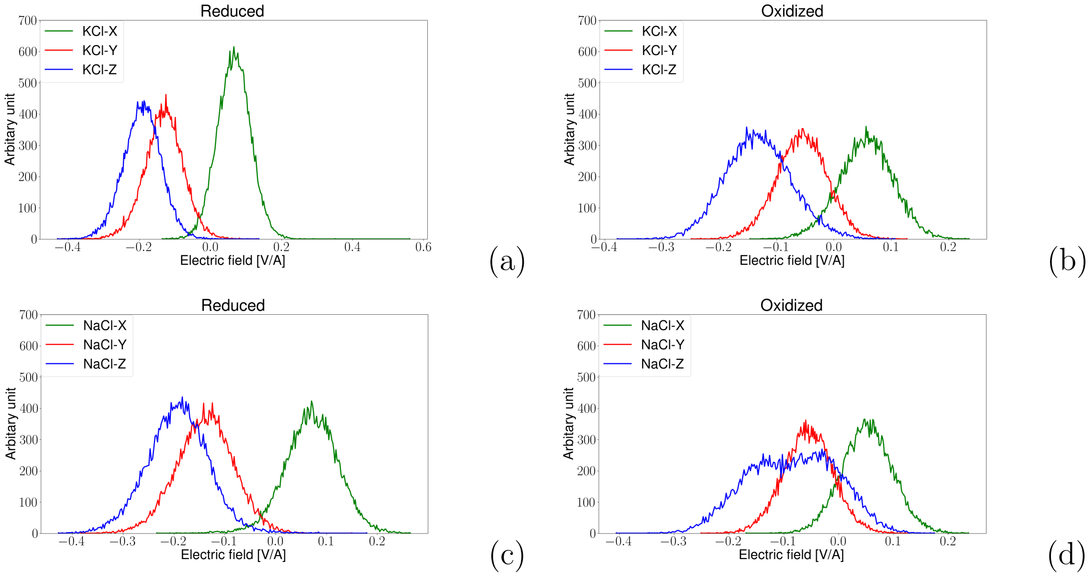

Figure S2: Histograms of the local electric field components [V/Å] at the Cu atom in the (a) reduced azurin in KCl solution, (b) oxidized azurin in KCl solution, (c) reduced azurin in NaCl solution, and (d) oxidized azurin in NaCl solution. The E_x, E_y, and E_z field components are shown in green, red, and blue, respectively.

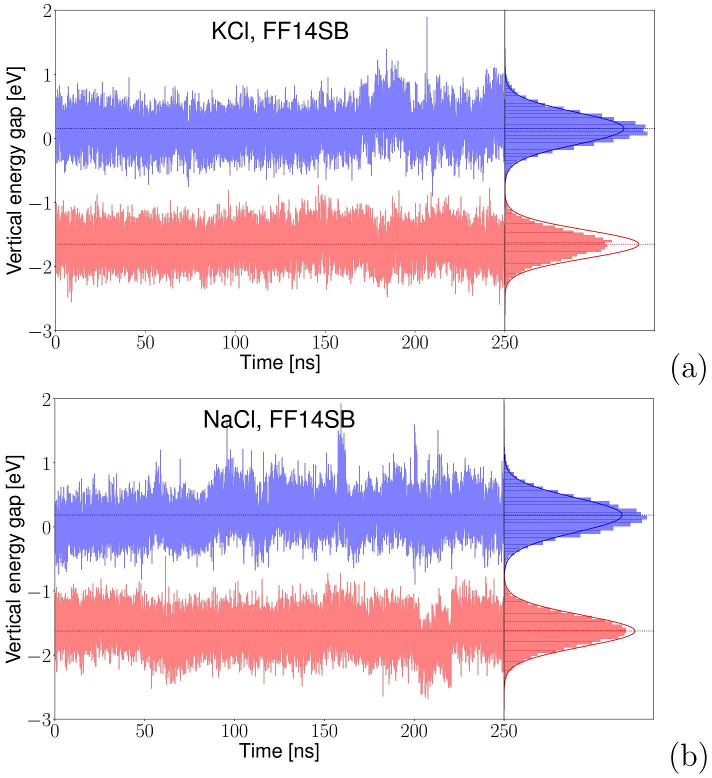

Figure S3: Local electric fields for a) reduced and b) oxidized azurin in an aqueous solution. Sulfur, oxygen, nitrogen, and copper atoms are highlighted as yellow, red, blue, and orange, respectively. The electric fields are illustrated as green and magenta for KCl and NaCl solutions, respectively.

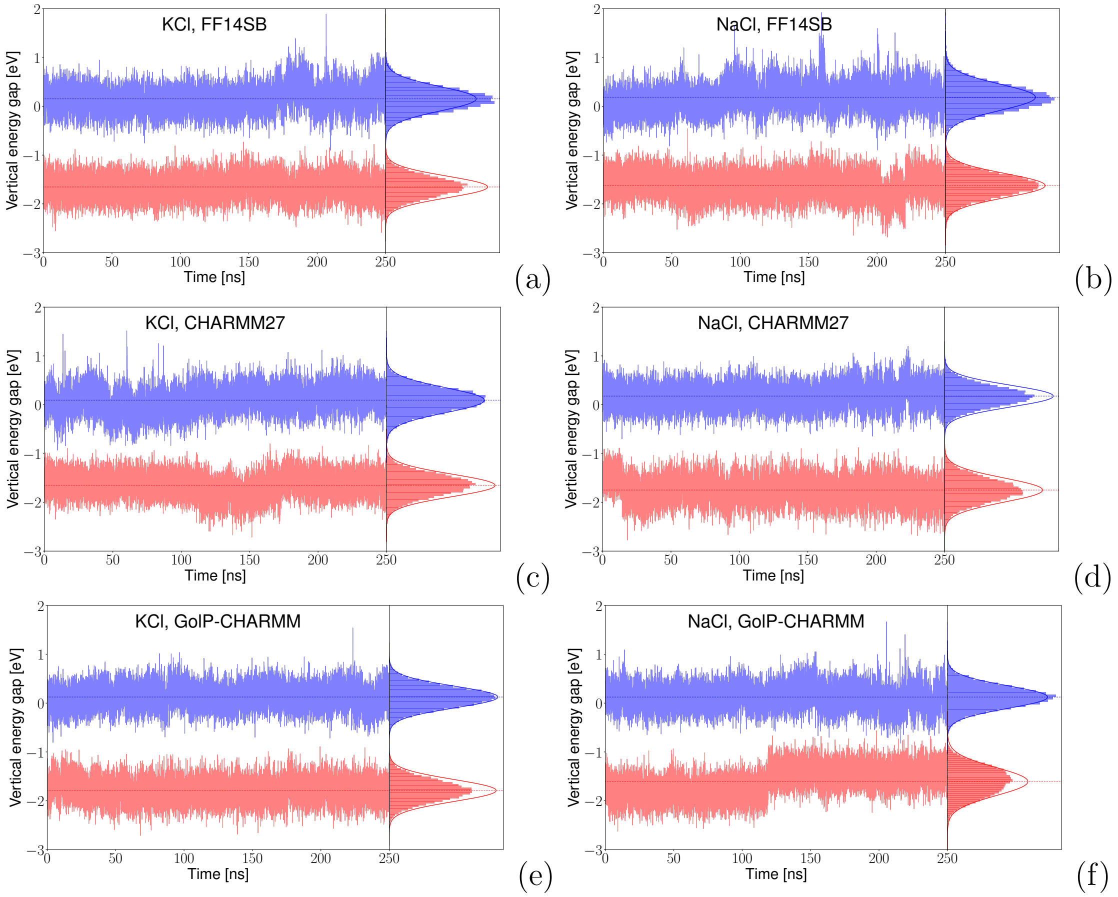

Figure S4: Vertical ionization energy (ΔE) values [eV] obtained by PMM on the sampled reduced (blue) and oxidized (red) azurin trajectories in NaCl and KCl aqueous solutions. Simulations performed in Amber FF14SB, CHARMM27, and GolP-CHARMM are compared. Histograms of the ΔE time series and the corresponding Gaussian distributions are shown on the right-hand side of the figures.

Table S1: The inner-part contributions of reorganization free energies [eV] for different quantum centres (QC) computed at the force field (FF) and density functional theory (DFT) levels. The energies were evaluated on the unperturbed QC geometries (FF values, calculated by ZINDO) and on the DFT-optimized QC configurations.

	FF	DFT
QC-3	0.02	0.12
QC-4	0.03	0.19
QC-5	0.03	0.25
QC-6	0.26	0.20

Table S2: Strength of local electric field with respect to the copper atom. The values are gained from MD calculations with GolP-CHARMM force field. All values are given in mV/Å. The electric fields in solution are also shown in Figure S3.

		Red	Ox
KCl solution	QC-5	250.50	168.40
NaCl solution	QC-5	246.95	110.84
Vac	QC-3	243.02	172.04
Vac	QC-4	257.02	79.84
Vac	QC-5	238.33	63.41
Vac	QC-6	218.89	72.57
S1	QC-5	216.53	145.77
S2	QC-5	198.99	202.72

2 Azurin in vacuum

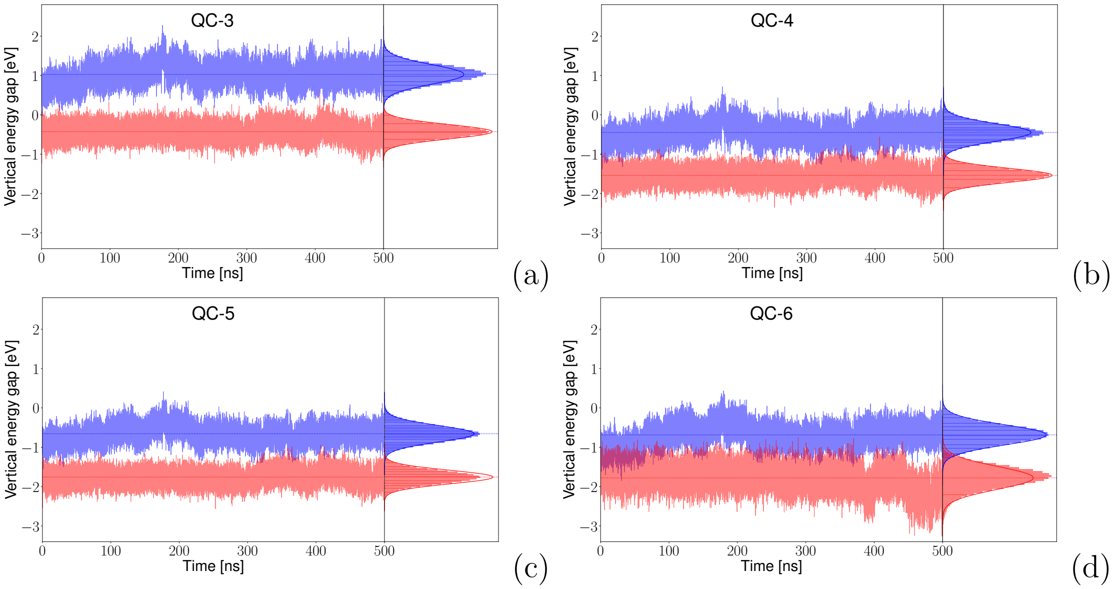

Figure S5: Vertical ionization energy (ΔE) values [eV] on the sampled reduced (blue) and oxidized (red) azurin trajectories in vacuum, computed on (a) QC-3, (b) QC-4, (c) QC-5, and (d) QC-6 quantum centres. The 70 excited state energies for Hamiltonian were obtained by ZINDO. 100000 MD samples were used. Histograms of the ΔE time series and the corresponding Gaussian distributions are shown on the right-hand side of the figures.

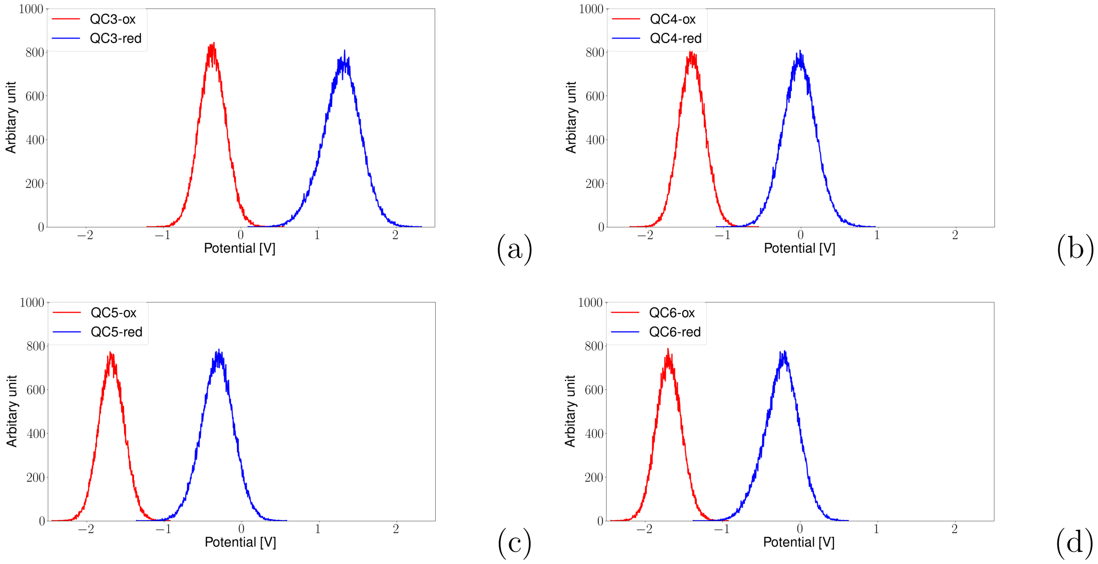

Figure S6: Histograms of the electrostatic potential [V] at the Cu atom in the reduced (blue) and oxidized (red) azurin in vacuum. Four different quantum centres are shown as a) QC-3, b) QC-4, c) QC-5, and d) QC-6. The potentials originate from the atomic point charges in the MM part of the model, i.e., the protein matrix, as defined in the GolP-CHARMM force field.

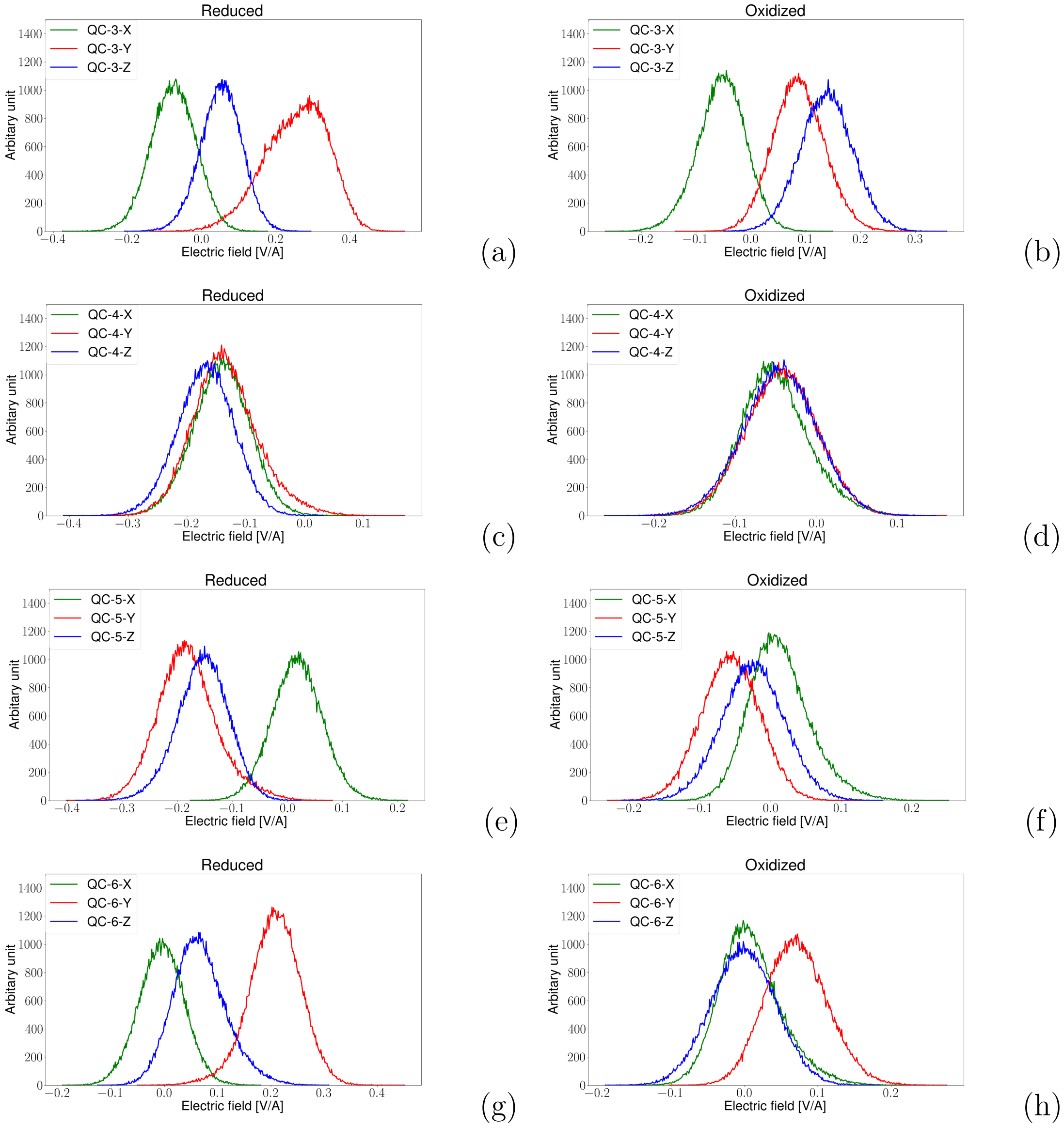

Figure S7: Histograms of the electric field components E_x, E_y, E_z [V/Å] at the Cu atom for azurin in vacuum in both reduced (left) and oxidized (right) states using different quantum centre partitioning (QC-3, QC-4, QC-5, and QC-6).

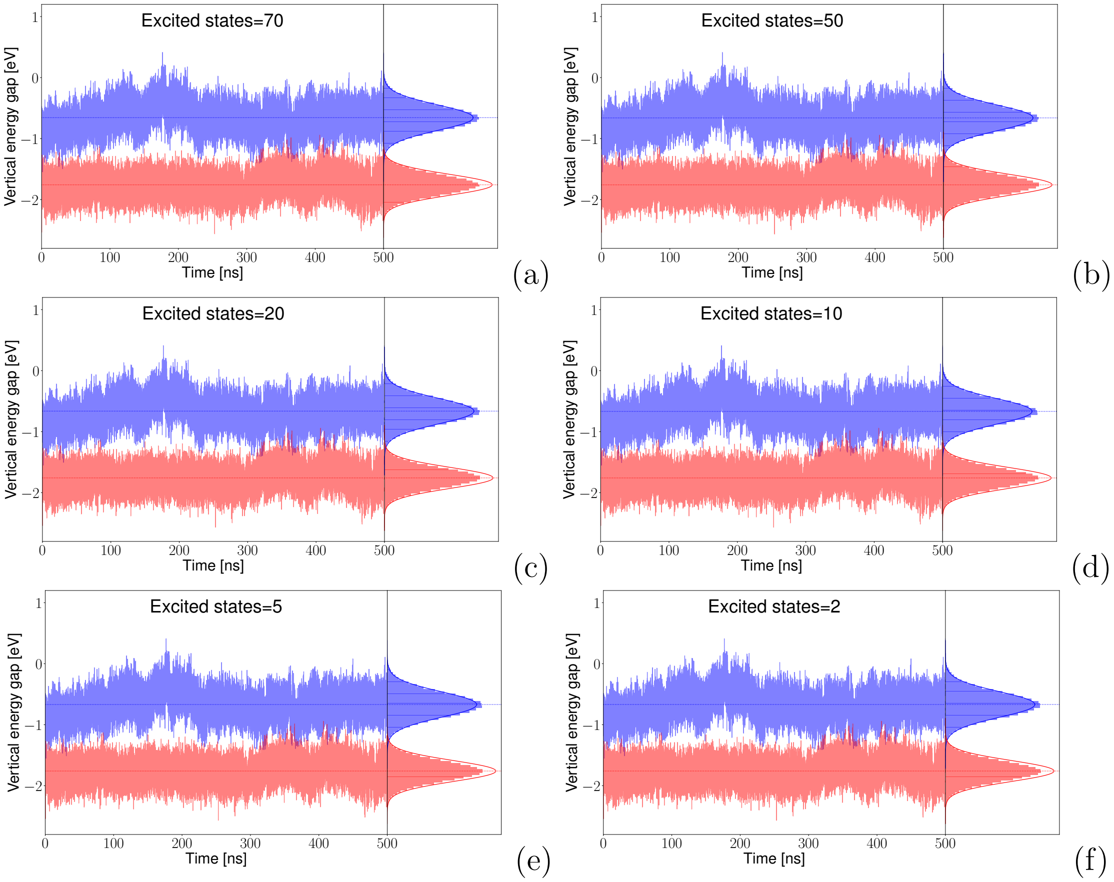

Figure S8: Vertical ionization energy (ΔE) values [eV] on the sampled reduced (blue) and oxidized (red) azurin trajectories in vacuum, computed with (a) 70, (b) 50, (c) 20, (d) 10, (e) 5, and (f) 2 excited states for PMM Hamiltonian. The excited states are gained through ZINDO calculations with QC-5 partitioning. Histograms of the ΔE time series and the corresponding Gaussian distributions are shown on the right-hand side of the figures.

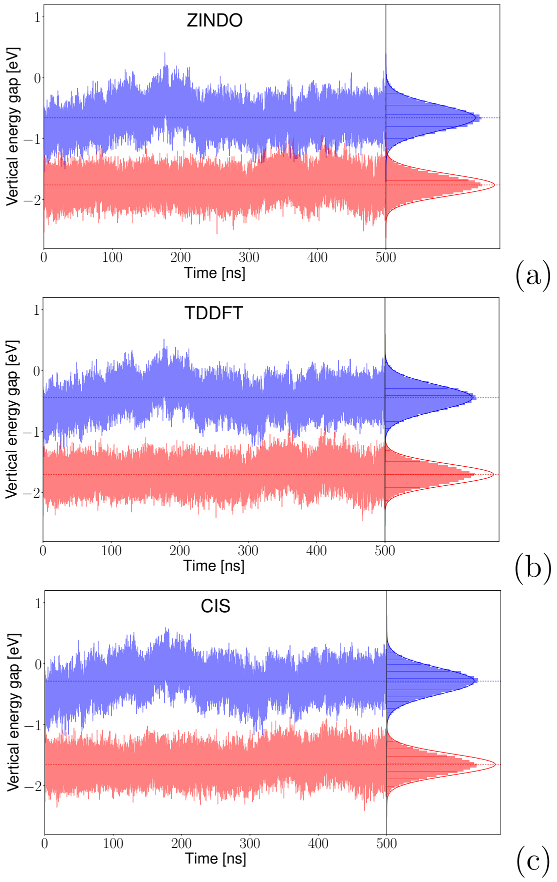

Figure S9: Vertical ionization energy (ΔE) values [eV] on the sampled reduced (blue) and oxidized (red) azurin trajectories in vacuum. The excited state energies were computed by (a) ZINDO, (b) TDDFT, and (c) CIS with QC-5 partitioning. For TDDFT and ZINDO, 70 excited states were used, while 40 excited states were used for CIS. Histograms of the ΔE time series and the corresponding Gaussian distributions are shown on the right-hand side of the figures.

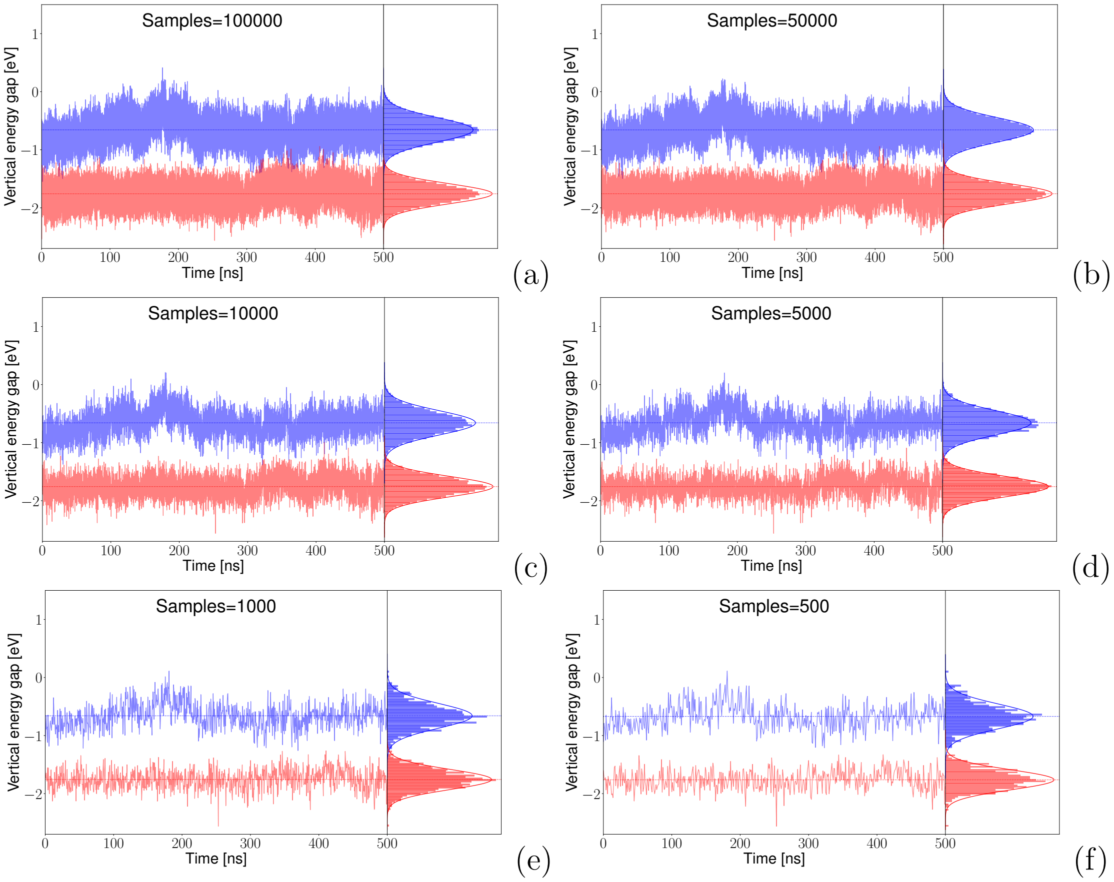

Figure S10: Vertical ionization energy (ΔE) values [eV] on the sampled reduced (blue) and oxidized (red) azurin trajectories in vacuum. The time series with (a) 100000, (b) 50000, (c) 10000, (d) 5000, (e) 1000, and 500 samples are compared. In all cases, QC-5 is selected as a quantum centre, and 70 excited states are computed through ZINDO method. Histograms of the ΔE time series and the corresponding Gaussian distributions are shown on the right-hand side of the figures.

Table S3: Mean value of vertical energy gap $\langle \Delta E \rangle_M$ (M = Red/Ox), average energy-gap fluctuations $\langle \delta E \rangle_M$, variational reorganization free energy λ_M^{var}, and Stokes reorganization free energy λ^{St} for azurin in vacuum. The values for different number of excited states N_{ES} on QC-3, QC-4, QC-5, and QC-6 structures are compared. All values are given in eV and λ^{St} is scaled by 1.35.

	N_{ES}	$\langle \Delta E \rangle_M$		$\langle \delta E \rangle_M$		λ_M^{var}		λ^{St}
		Red	Ox	Red	Ox	Red	Ox	
QC-3	10	1.02	-0.46	0.25	0.18	0.97±0.01	0.58±0.004	0.66±0.002
	20	1.02	-0.43	0.25	0.18	0.97±0.01	0.58±0.004	0.64±0.002
	50	1.03	-0.43	0.25	0.18	0.97±0.01	0.58±0.004	0.65±0.002
	70	1.03	-0.43	0.25	0.18	1.00±0.01	0.60±0.004	0.66±0.002
QC-4	10	-0.46	-1.54	0.22	0.18	0.88±0.01	0.63±0.004	0.57±0.002
	20	-0.46	-1.54	0.22	0.18	0.87±0.01	0.63±0.004	0.57±0.002
	50	-0.45	-1.54	0.22	0.18	0.87±0.01	0.63±0.004	0.57±0.002
	70	-0.45	-1.54	0.22	0.18	0.90±0.01	0.65±0.004	0.57±0.002
QC-5	2	-0.66	-1.76	0.21	0.17	0.88±0.01	0.67±0.004	0.63±0.002
	5	-0.66	-1.76	0.21	0.17	0.88±0.01	0.67±0.004	0.63±0.002
	10	-0.67	-1.76	0.21	0.17	0.85±0.01	0.65±0.004	0.63±0.002
	20	-0.66	-1.76	0.21	0.17	0.85±0.01	0.65±0.004	0.63±0.002
	50	-0.66	-1.76	0.21	0.17	0.85±0.01	0.65±0.004	0.63±0.002
	70	-0.66	-1.76	0.21	0.17	0.87±0.01	0.66±0.004	0.63±0.002
QC-6	10	-0.70	-1.78	0.26	0.29	0.95±0.01	1.23±0.01	0.41±0.003
	20	-0.69	-1.78	0.26	0.29	0.95±0.01	1.23±0.01	0.42±0.003
	50	-0.69	-1.78	0.25	0.29	0.95±0.01	1.32±0.01	0.42±0.003
	70	-0.69	-1.78	0.25	0.29	0.98±0.01	1.26±0.01	0.42±0.003

Table S4: Mean value of vertical energy gap $\langle \Delta E \rangle_M$ (M = Red/Ox), average energy-gap fluctuations $\langle \delta E \rangle_M$,variational reorganization free energy λ_M^{var}, and Stokes reorganization free energy λ^{St} for azurin in vacuum. The values for different levels of the theory used for the QC treatment are compared. All values are given in eV and λ^{St} is scaled by 1.35.

Method	$\langle \Delta E \rangle_M$		$\langle \delta E \rangle_M$		λ_M^{var}		λ^{St}
	Red	Ox	Red	Ox	Red	Ox	
ZINDO	-0.66	-1.76	0.21	0.17	0.87±0.01	0.66±0.004	0.63±0.002
TDDFT	-0.16	-1.63	0.23	0.18	0.96±0.01	0.69±0.004	0.75±0.002
CIS	-0.29	-1.66	0.22	0.17	0.91±0.01	0.71±0.004	0.73±0.002

Table S5: Mean value of vertical energy gap $\langle \Delta E \rangle_M$ (M = Red/Ox), average energy-gap fluctuations $\langle \delta E \rangle_M$,variational reorganization free energy λ_M^{var}, and Stokes reorganization free energy λ^{St} for azurin in vacuum. The values are compared for different numbers of MD samples. All values are given in eV and λ^{St} is scaled by 1.35.

N_{samples}	$\langle \Delta E \rangle_M$		$\langle \delta E \rangle_M$		λ_M^{var}		λ^{St}
	Red	Ox	Red	Ox	Red	Ox	
500	-0.67	-1.75	0.21	0.24	0.88±0.07	1.03±0.05	0.62±0.02
1000	-0.66	-1.75	0.21	0.24	0.87±0.05	1.04±0.04	0.63±0.02
5000	-0.66	-1.75	0.21	0.22	0.84±0.02	0.90±0.03	0.63±0.01
10000	-0.66	-1.75	0.21	0.22	0.85±0.02	0.89±0.02	0.63±0.01
50000	-0.66	-1.75	0.21	0.22	0.85±0.01	0.90±0.01	0.63±0.002
100000	-0.66	-1.76	0.21	0.17	0.87±0.01	0.66±0.004	0.63±0.002

3 Azurin adsorbed on gold

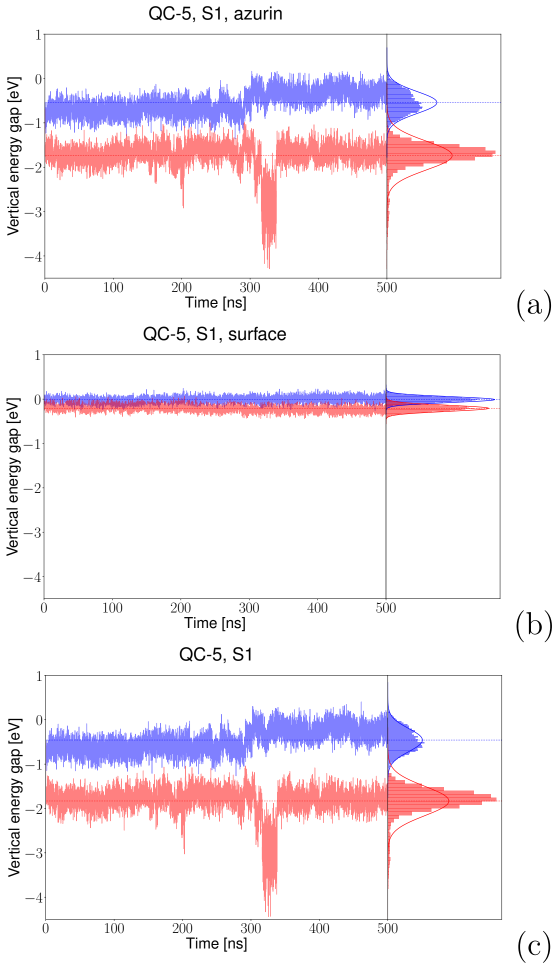

Figure S11: Vertical ionization energy (ΔE) values [eV] on the sampled reduced (blue) and oxidized (red) azurin trajectories in the **S1** adsorption structure. The contributions from (a) protein, (b) gold surface, and (c) for the total adsorbed system are shown. The QC-5 partition was used, and the 70 excited state energies for Hamiltonian were obtained by ZINDO. 10000 samples were used from MD calculations. Histograms of the ΔE time series and the corresponding Gaussian distributions are shown on the right-hand side of the figures.

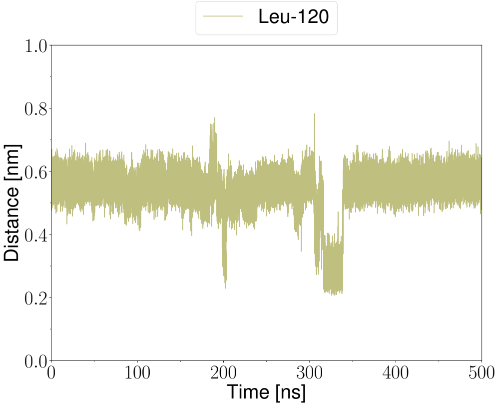

Figure S12: Tracked O(Leu120)-Cu distance during the MD simulation of the oxidized **S1** adsorption azurin structure on the gold surface.

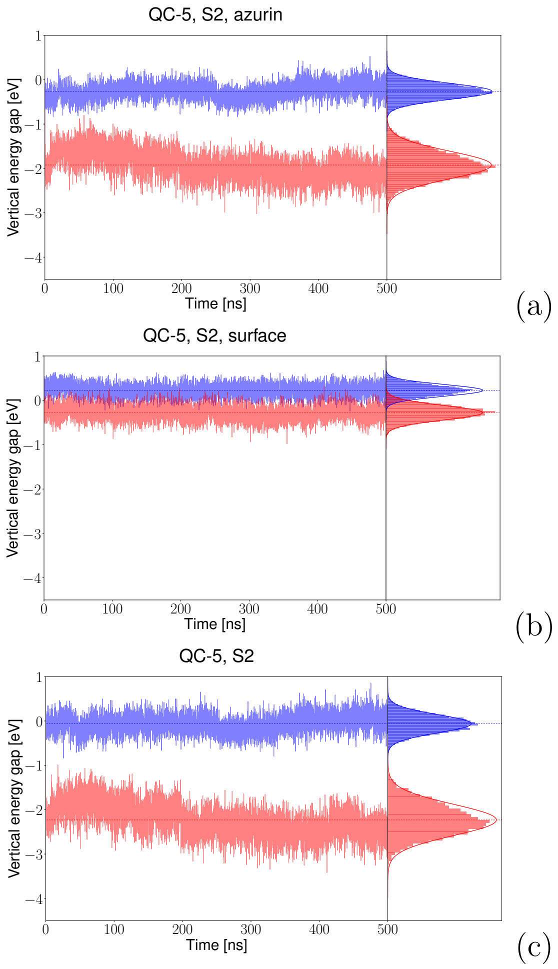

Figure S13: Vertical ionization energy (ΔE) values [eV] on the sampled reduced (blue) and oxidized (red) azurin trajectories in the **S2** adsorption structure. The contributions from (a) protein, (b) gold surface, and (c) for the total adsorbed system are shown. The QC-5 was used in combination with 70 excited states calculated using ZINDO. 10000 samples were collected from the MD calculations. Histograms of the ΔE time series and the corresponding Gaussian distributions are shown on the right-hand side of the figures.

Table S6: Mean value of vertical energy gap $\langle \Delta E \rangle_M$ (M = Red/Ox), average energy-gap fluctuations $\langle \delta E \rangle_M$, variational reorganization free energy λ_M^{var}, and Stokes reorganization free energy λ^{St} for the **S1** and **S2** adsorption structures. Calculations were performed using QC-5 partitioning, ZINDO method with 70 excited states, and 10000 MD samples. The total values and contributions from azurin and gold surface are shown. All values are given in eV.

	N_{Moiety}	$\langle \Delta E \rangle_M$		$\langle \delta E \rangle_M$		λ_M^{var}		λ^{St}
		Red	Ox	Red	Ox	Red	Ox	
S1	Azurin	-0.54	-1.73	0.25	0.32	1.13±0.02	1.78±0.04	0.67±0.01
	Gold	-0.01	-0.21	0.07	0.07	0.10±0.002	0.10±0.002	0.07±0.02
	Total	-0.46	-1.83	0.26	0.33	1.23±0.03	1.85±0.04	0.74±0.01
S2	Azurin	-0.26	-1.92	0.18	0.31	0.69±0.01	1.60±0.04	0.84±0.01
	Gold	0.22	-0.28	0.13	0.16	0.25±0.01	0.38±0.01	0.19±0.004
	Total	-0.06	-2.23	0.20	0.35	0.82±0.02	2.00±0.05	1.13±0.01

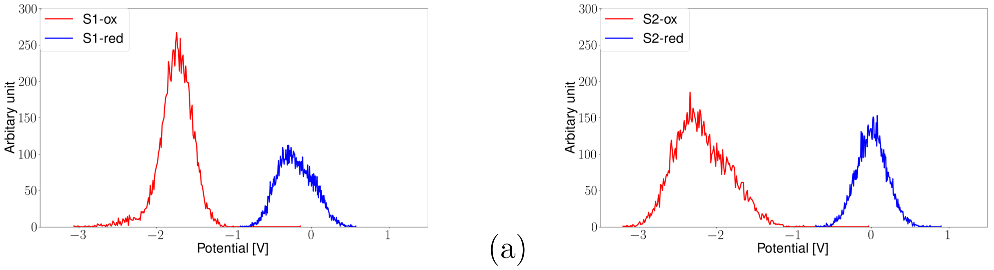

(a) (b)

Figure S14: Histograms of the electrostatic potential [V] at the Cu atom in the reduced (blue) and oxidized (red) azurin adsorbed onto the gold surface in (a) **S1** and (b) **S2** geometries. The potentials originate from the atomic point charges in the MM part of the model, i.e., the protein matrix and the gold surface, as defined in the GolP-CHARMM force field.

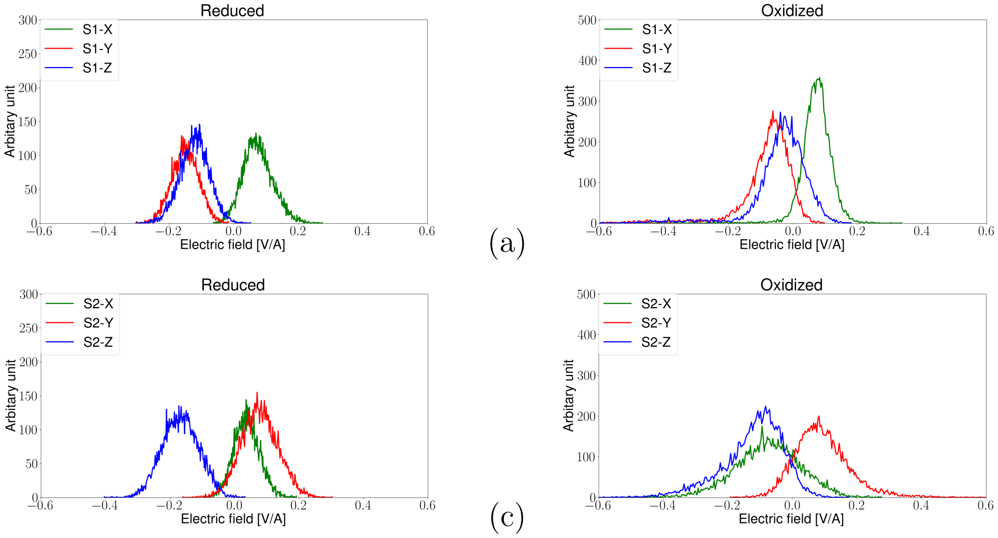

(a) (b) (c) (d)

Figure S15: Histograms of the electric field components [V/Å] fixated at the Cu atom for a-b) **S1** and c-d) **S2** azurin structures adsorbed on gold in reduced (left) and oxidized (right) states. The field components E_x, E_y, E_z are shown in green, red, and blue, respectively.

4 Azurin junction

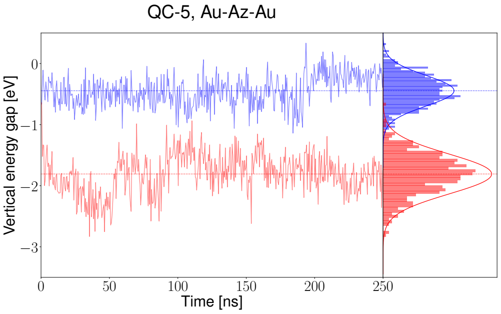

Figure S16: Vertical ionization energy (ΔE) values [eV] on 500 MD samples taken from trajectories of reduced (blue) and oxidized (red) azurin junction structure. The QC-5 partition and 70 ZINDO states were used. Histograms of the ΔE time series and the corresponding Gaussian distributions are shown on the right-hand side of the figures.

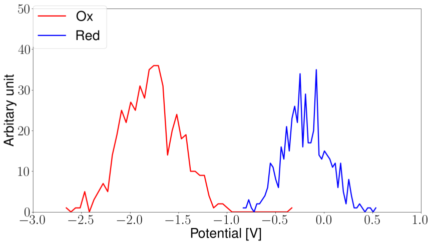

Figure S17: Histograms of the electrostatic potential [V] at the Cu atom in the reduced (blue) and oxidized (red) azurin junction. The potentials originate from the atomic point charges in the MM part of the model, i.e., the protein matrix and the gold surfaces, as defined in the GolP-CHARMM force field.

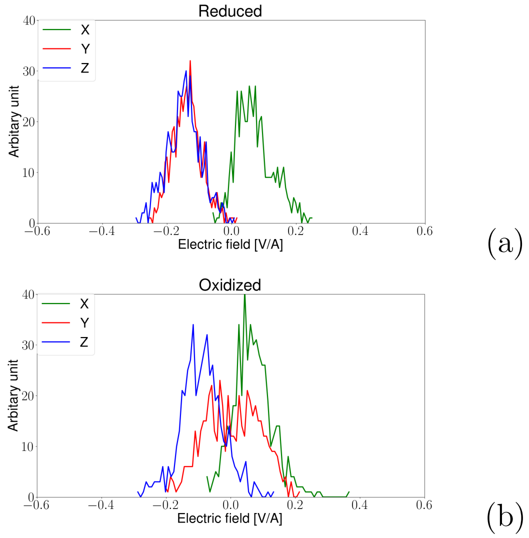

Figure S18: Histograms of the electric field components [V/Å] fixated at the Cu atom for (a) reduced and (b) oxidized azurin junction. The field components E_x, E_y, E_z are shown in green, red, and blue, respectively.

5 Statistical errors

Table S7: The comparison between QM/MM and PMM values of reorganization free energies (variational λ_M^{var}, $M = \{\text{Red, Ox}\}$ and Stokes λ^{St}) and their statistical error in *aqueous solution with NaCl*. The QM/MM values are evaluated on 500 samples while 25000 were processed in PMM (using QC-5 partitioning and 100 states obtained by ZINDO).

Force field	QM/MM			PMM		
	$\lambda_{\text{Red}}^{\text{var}}$	$\lambda_{\text{Ox}}^{\text{var}}$	λ^{St}	$\lambda_{\text{Red}}^{\text{var}}$	$\lambda_{\text{Ox}}^{\text{var}}$	λ^{St}
FF14SB	0.81±0.08	0.67±0.07	0.63±0.02	1.04±0.02	0.89±0.01	0.74±0.01
CHARMM27	0.71±0.07	0.67±0.06	0.67±0.02	0.79±0.01	0.92±0.01	0.77±0.004
GolP-CHARMM	0.71±0.07	0.79±0.07	0.68±0.02	0.83±0.01	1.15±0.02	0.71±0.004

Table S8: The comparison between QM/MM and PMM values of reorganization free energies (variational λ_M^{var}, $M = \{\text{Red, Ox}\}$ and Stokes λ^{St}) and their statistical error in *aqueous solution with KCl*. The QM/MM values are evaluated on 500 samples while 25000 were processed in PMM (using QC-5 partitioning and 100 states obtained by ZINDO).

Force field	QM/MM			PMM		
	$\lambda_{\text{Red}}^{\text{var}}$	$\lambda_{\text{Ox}}^{\text{var}}$	λ^{St}	$\lambda_{\text{Red}}^{\text{var}}$	$\lambda_{\text{Ox}}^{\text{var}}$	λ^{St}
FF14SB	0.64±0.07	0.68±0.07	0.66±0.02	0.92±0.02	0.78±0.01	0.73±0.004
CHARMM27	0.94±0.09	0.62±0.06	0.64±0.02	0.80±0.02	0.82±0.01	0.72±0.004
GolP-CHARMM	0.76±0.07	0.56±0.05	0.65±0.02	0.78±0.01	0.80±0.01	0.77±0.004

Table S9: The comparison between QM/MM and PMM values of reorganization free energies (variational λ_M^{var}, $M = \{\mathrm{Red, Ox}\}$ and Stokes λ^{St}) and their statistical error in *vacuum*. The QM/MM values are evaluated on 500 samples while 100000 were processed in PMM (using QC-5 partitioning and 70 states obtained by ZINDO).

QM/MM			PMM		
$\lambda_{\mathrm{Red}}^{\mathrm{var}}$	$\lambda_{\mathrm{Ox}}^{\mathrm{var}}$	λ^{St}	$\lambda_{\mathrm{Red}}^{\mathrm{var}}$	$\lambda_{\mathrm{Ox}}^{\mathrm{var}}$	λ^{St}
1.33±0.12	0.64±0.06	0.65±0.02	0.87±0.01	0.66±0.004	0.63±0.002

Table S10: The comparison between QM/MM and PMM values of reorganization free energies (variational λ_M^{var}, $M = \{\mathrm{Red, Ox}\}$ and Stokes λ^{St}) and their statistical error on the *gold (111) surfaces*. The QM/MM values are evaluated on 500 samples while 10000 were processed in PMM (using QC-5 partitioning and 70 states obtained by ZINDO).

Structure	QM/MM			PMM		
	$\lambda_{\mathrm{Red}}^{\mathrm{var}}$	$\lambda_{\mathrm{Ox}}^{\mathrm{var}}$	λ^{St}	$\lambda_{\mathrm{Red}}^{\mathrm{var}}$	$\lambda_{\mathrm{Ox}}^{\mathrm{var}}$	λ^{St}
S1	1.18±0.11	1.29±0.12	0.56±0.03	1.23±0.03	1.85±0.04	0.74±0.01
S2	1.00±0.09	1.13±0.10	0.90±0.03	0.84±0.02	2.07±0.05	1.03±0.01